Optical redshift in the Raman scattering spectra of Fe-doped multiwalled carbon nanotubes: Experiment and theory

G. M. Bhalerao,[1,2] M. K. Singh,[3] A. K. Sinha,[1] and Haranath Ghosh[1]

[1]*Indus Synchroton Utilization Division, Raja Ramanna Center for Advanced Technology, Indore, Madhya Pradesh IN-452013, India*

[2]*UGC-DAE-CSR, Kalpakkam Node, Tamil Nadu-603104, India*

[3]*Laser Material Development and Devices Division, Raja Ramanna Center for Advanced Technology, Indore, Madhya Pradesh IN-452013, India*

(Received 12 December 2011; revised manuscript received 26 June 2012; published 11 September 2012)

Electron doping of arc-grown multiwalled carbon nanotubes coated with iron nanoparticles is established by the *redshift* of the graphite peak and a larger redshift of the defect peak in the Raman spectra of doped samples compared to the corresponding peak positions in undoped samples. This is unlike the *blue Raman shift* usually observed in defect-induced double-Raman-resonance studies. On doping, the defect peak splits into two peaks. One has approximately the same dispersion (50 $cm^{-1}\,eV^{-1}$) as the defect peak of undoped samples. The other peak has a very large dispersion (110 $cm^{-1}\,eV^{-1}$). We show that the above observations are consequences of drastic changes in the electronic band structure of the graphitic systems under doping. Experimental observations of the splitting of the defect peak into two and larger dispersions of one of the peaks are explained via double-Raman-resonance processes studied through detailed theoretical calculations of electronic and phonon band structures based on a first principles *ab initio* method.

DOI: 10.1103/PhysRevB.86.125419 PACS number(s): 78.67.Ch, 78.30.Na, 78.67.Bf

I. INTRODUCTION

Scientific interest in graphite was recently stimulated by a report of the massless and relativistic properties of the conduction electrons in a single graphene layer that are responsible for the unusual property of the quantum Hall effect in this system.[1] Inspired by the Nobel-Prize-winning creation of the carbon material graphene, atom-thin sheets of silicon, termed silicene, have been discovered that are expected to have all the above-mentioned rich physics as in graphene but perhaps may be even more accessible.[2,3] Raman spectroscopy has played an important role in the structural characterization of graphitic materials such as pyrolytic graphite, carbon fibers, nanographite ribbons, fullerenes, and carbon nanotubes.[4] Given that there are strong similarities in the electronic band structures between graphene and silicene,[3] doping-dependent Raman studies of one class of materials should provide important insight into the other class. Instead of electron-donating materials, transition metals, in particular Fe, have recently been used as catalysts in the growth of multiwalled carbon nanotubes. Therefore, a detailed, systematic study of the interaction of Fe on multiwalled carbon nanotubes is called for.

In this paper, we present a combined experimental and theoretical understanding of the study of the doping-dependent Raman shift in multiwalled carbon nanotubes (MWCNTs). In particular, we show conclusively that the doping-induced defect peak is *redshifted* compared to the defect peaks in undoped samples. This is qualitatively *different* from the defect-induced blue Raman shift.[5] Electron doping of arc-grown MWCNTs coated with iron nanoparticles has been established by the redshift of the graphite peak (G peak) and a larger redshift of the defect peak (D peak) in the Raman spectra of doped samples compared to the corresponding peak positions in undoped samples. Defects in MWCNTs cause "defect scattering," which introduces a violation of $q = 0$ conservation and gives rise to a D peak. A further increase of this defect allows scattering with a larger momentum transfer, causing a blue Raman shift because of the nature of the phonon dispersion around the K point. A large redshift in the D peak along with an experimentally observed increase in the defect density is contradictory to the expected blueshift. It is further observed that, on doping, the D peak splits in two. One of the peaks, assigned as D_2, has nearly the same dispersion as the D peak of the undoped sample. The other peak, assigned as D_1, has a larger dispersion. A redshift in the G peak of the order of 8 cm^{-1} is observed in our Raman measurement, suggesting modification of the elastic-force constants. Even up to 20% modification in the force constants in the model calculations[4] cannot account for the shift in the D peak whereas the redshift in the G peak can be completely accounted for on the basis of the phonon alone. This together with the observation of the splitting of the defect peak under doping suggests that the origin of our observations is due to the change in the electronic band structure as well as the change in the Raman-active-phonon dispersions. This understanding has been achieved through the detailed theoretical *ab initio* studies on electronic band structures and phonon dispersions of doped and undoped graphites.

Apart from disorder-induced $D_{1,2}$ Raman features, two phonon G' modes (the overtone of the D mode) are always Raman allowed even in defect-free conditions.[6] The dynamics of the G' mode with substitutional dopants such as P and N is studied experimentally in low-dimensional single-walled carbon nanotubes (SWCNTs). In contrast, we show that the doping of a transition metal (Fe) in MWCNTs causes preferential doping (thereby making inequivalent graphene layers) and increases the defect density. The dynamics of the G' mode in SWCNTs or even in graphene with substitutional impurities is explained through phonon renormalization caused by the Kohn anomaly.[6] The phonon self-energy in a low-dimensional semimetallic system such as SWCNTs or graphene results in a Lindhard function which exhibits a logarithmic singularity

[due to electron-hole symmetry, also known as the nesting property of a Fermi surface (FS)], causing phonon softening at $q = 2k$ (i.e., both the electronic states k and $k + q$ involved in the double-resonance process fall on the FS, see below) and hence the Kohn anomaly. However, we show that in MWCNTs, due to preferential doping with Fe, which causes drastic changes in the electronic band structure, the nesting property no longer exists, and both the k and the $k + q$ state may not fall together on the FS. Therefore, the Kohn anomaly in Fe-doped MWCNTs is expected to be weaker or absent, indicating a possibly different origin of phonon renormalization. Thus, the mechanism of the observed red Raman shift in the D_1 peak is unique; it is of electronic origin, and the phonon renormalization (the change in the slope of the phonon dispersion) is an indirect effect.

II. EXPERIMENTAL METHODS AND RESULTS

Electron doping in electric arc-grown MWCNTs, used in the present study, is obtained by dispersing CNTs in a mixture of iron precursor, similar to the one used to grow iron-oxide nanoparticles,[7] and by then utilizing thermolysis (400 °C) and subsequent annealing after the separation of iron-coated MWCNTs magnetically. Raman data are taken at room temperature in back-reflection geometry at 633- and 488-nm excitation wavelengths (λ_{ex}). All the Raman spectra were recorded at a laser power of 9 mW and were repeated between 0.9 to 9 mW to ensure no heating effects. In order to ensure that there was no heating effect due to the laser, some of the measurements were repeated at laser powers between 0.9 and 9 mW wherein no peak shift was obtained.

The detailed Raman spectra obtained are presented in Fig. 1. Two pronounced peaks, one between 1572 and 1582 cm^{-1} called the G (graphite) peak and the other between 1300 and 1332 cm^{-1} called the D (defect) peak, are present in these

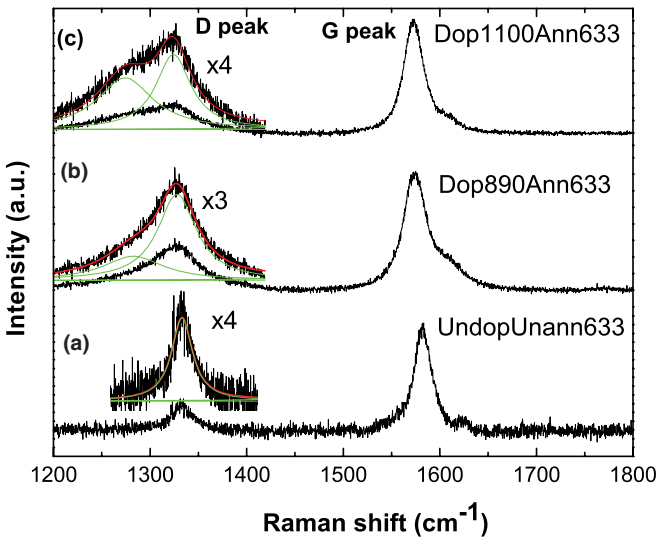

FIG. 1. (Color online) Raman spectra of CNTs (a) undoped and unannealed, (b) iron-doped and annealed at 890 °C, and (c) iron-doped and annealed at 1100 °C, taken at 633 nm. D peaks are shown magnified with colored, smooth lines representing (a) single-Lorentzian and (b) and (c) double-Lorentzian peak fitting.

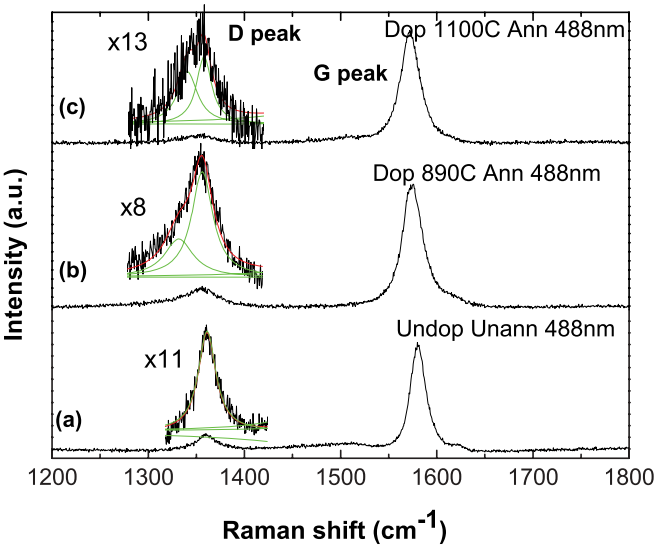

FIG. 2. (Color online) Raman spectra of CNTs (a) undoped and unannealed, (b) iron-doped and annealed at 890 °C, and (c) iron-doped and annealed at 1100 °C, taken at 488 nm. D peaks are shown magnified with colored lines representing (a) single-Lorentzian and (b) and (c) double-Lorentzian peak fitting.

spectra. The D peak is a mode of A_{1g} symmetry involving phonons near the K point at the zone boundary of graphite.[4] This mode is forbidden in the defect-free lattice of graphite. The ratio (of intensities of the defect to the G peak) I_D/I_G is used to quantify the defects in graphite and CNT samples.[8] In addition, the D-peak position changes with λ_{ex}. Therefore, its position 1332 cm^{-1} at $\lambda_{ex} = 633$ nm is in agreement with earlier studies.[9] The Raman spectra for all the samples are analyzed to obtain the peak positions, the peak widths, and peak areas, using Lorentzian-peak-fit profiles. A marked difference in the D peak is observed on doping and subsequent annealing at 890 and 1100 °C. A double-Lorentzian-peak fit is necessary for the appropriate representation of the D peak as shown in Fig. 1.

Raman spectra for the same three samples are presented in Fig. 2 for lower λ_{ex} (488 nm). We again obtain similar observations for this λ_{ex}. The positions of the D peak for the undoped sample and the D_1 and D_2 peaks in Fe-doped samples are plotted in Fig. 3.

The following observations are made from the detailed analysis of the peak positions. (1) The behavior of the D peak is strongly influenced by doping; a well-defined symmetric D peak in undoped CNTs [cf. Figs. 1(a) and 2(a)] becomes broader and asymmetric for the doped CNTs when annealed at 890 °C [cf. Figs. 1(b) and 2(b)]. The D peak further broadens, and asymmetry increases as the annealing temperature is increased to 1100 °C [cf. Figs. 1(c) and 2(c)]. On iron coating and subsequent annealing, the D peak splits in two as confirmed through the detailed analysis of the peak positions. D_1 is the redshifted peak (by 40 cm^{-1}), and D_2 is the normal peak corresponding to that of the undoped sample. (2) Comparison of Figs. 1 and 2 reveals that the dispersion in the D-peak position in the undoped sample is found to be $\simeq$50 cm^{-1}/eV in agreement with the literature.[9] The dispersion in the D_2-peak position is found to be about the

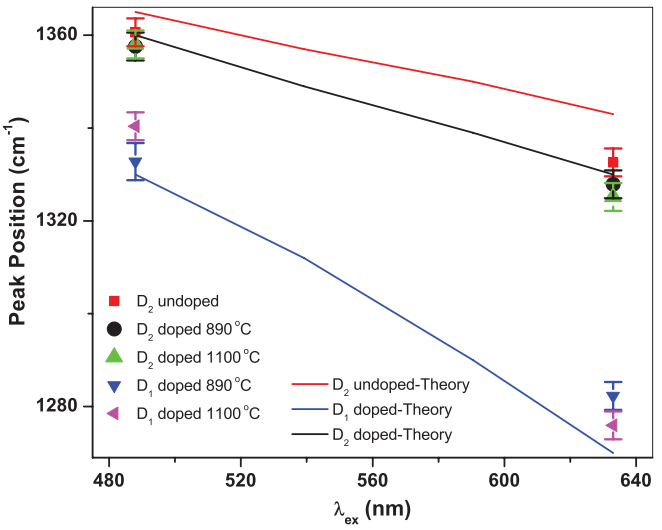

FIG. 3. (Color online) Raman-peak positions of $D_{1,2}$ peaks as a function of the laser-excitation wavelength (λ_{ex}) are shown. Solid lines are theoretical estimations of corresponding peak positions. Symbols (not joined by lines) with error bars are experimental data. Color codes are explained in the legend.

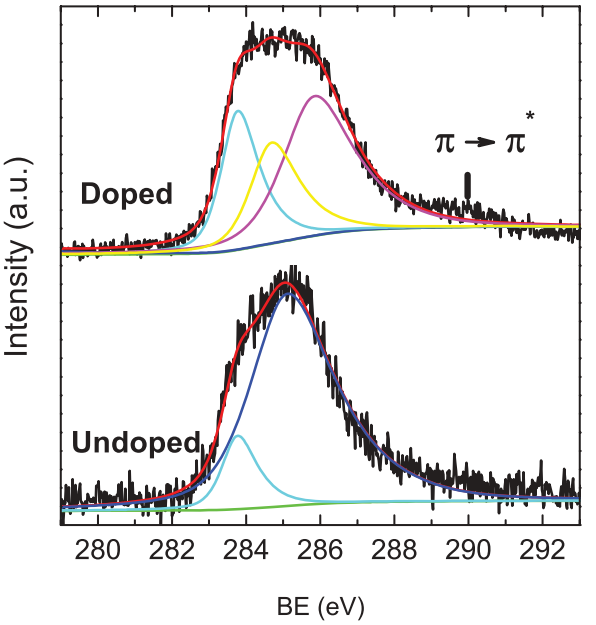

FIG. 4. (Color online) Carbon core-level XPS spectra of undoped and doped MWCNTs.

same as that of the D peak whereas that for the D_1 peak is found to be $\simeq$110 cm^{-1}/eV for the sample annealed at 890 °C, increasing slightly for the sample annealed at 1100 °C. We argue below that the observed change in the Raman spectra (G-peak and D-peak positions) upon Fe incorporation is a consequence of electron doping. (3) With 633-nm excitation, the G-peak position for the undoped CNTs is 1582 cm^{-1}, which shifts to 1574 and 1573 cm^{-1} for doped CNTs annealed at 890 and 1100 °C, respectively. The I_D/I_G ratios are 0.33, 0.9, and 0.82 for the three samples, respectively. The increase in the I_D/I_G ratio upon annealing shows an increase in structural defects in agreement with our earlier studies.[10] The G peak is always due to $q = 0$ phonons at the Γ point of the two-dimensional (2D) Brillouin zone of graphite and does not change because of defects (see the last reference of Ref. 4). A redshift in the G-peak position has been observed because of n-type doping in double-walled carbon nanotubes (DWCNTs).[11] Graphite-intercalation compounds also show the redshift on n-type doping by alkali metals.[12] Therefore, we argue that the MWCNTs in the present study have also been n-type doped by Fe incorporation and annealing. The same conclusion is drawn based on the shift in the D-peak position on doping. The increase in the defect density alone blueshifts the D peak.[5] We see an increase in the defect density and a redshift in the D peak on Fe doping. This also suggests n-type doping in the sample. Doping is further confirmed by carbon core-level x-ray-photoelectron-spectroscopy (XPS) studies, using an Al $K\alpha$ source. The C 1s spectra thus obtained are shown in Fig. 4. Due to the asymmetric shape of the peak, a two-peak fit is performed, and the average value (284.5 eV) of the two peaks at 283.8 and 285.1 eV is in close agreement with the literature value for pristine graphite.[13] The presence of a moderate density of defects in undoped samples can cause acceptorlike states and give an additional peak at a lower binding energy.[14] Upon doping, a new component with large intensity appears at 285.8 eV with a shift of +1.3 eV as compared to the pristine value. This much of a shift in the binding energy of the core level is similar to that reported for graphite intercalated with K and C_{60} doped with Cs. K and Cs are strong electron-donor materials.[15] Fe doping results in two inequivalent graphene sheets as shown in Fig. 5, causing further splitting in the XPS signal as explained above. This is also the origin of the D-peak splitting in Raman studies. The discussions above qualitatively establish that Fe incorporation and subsequent annealing dopes n-type MWCNTs.

III. THEORETICAL CALCULATION

As mentioned earlier, the redshift of the G-peak position can be explained through changes in the elastic-force constants. We have modified the force constants by as much as 20% of the reported values (Saito *et al.*).[4] This, however, cannot explain the observed large redshift of the D peak as well as its splitting. In order to understand the above-mentioned experimental observations, we performed detailed density-functional-theory-based *ab initio* studies. We have employed

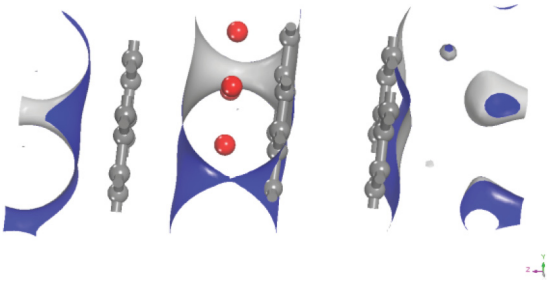

FIG. 5. (Color online) Fe doping in graphite. Gray is carbon, and red is Fe, clearly showing the charge transfer. The gray in isosurface-charge-density mapping shows the density inside the sphere, and the blue shows outside the sphere. The darker the color, the greater is the density.

the SIESTA code[16] to obtain optimized structures of graphite and Fe-doped graphite and their electronic and phonon dispersions within the generalized-gradient approximation (GGA).[17] The electron-ion interactions are represented by norm-conserving pseudopotentials, generated by the ATOM program included in the SIESTA code. The k-point separation is 0.0199 Å^{-1}, which corresponds to $24 \times 24 \times 8$ and $23 \times 23 \times 5$ Monkhorst-Pack k-point grids in the Brillouin zone of the primitive cells of graphite and Fe-doped graphite, respectively. The plane-wave cutoff of 550 eV is used for our calculations. We have employed the finite-displacement method to calculate the phonon dispersions of graphite and Fe-doped graphite. For this purpose, the supercell is defined by the cutoff radius which is 5 Å and which corresponds to 200 and 250 atoms in graphite and Fe-doped graphite, respectively. The displacement lengths are 0.02 Å in both cases. The optimized lattice constants of graphite are $a = 2.474$ Å and $c = 7.2$ Å. To study the effect of Fe doping in CNTs, we initially place an iron atom at the center of the carbon ring in the primitive cell of graphite, and the resulting structure is thoroughly optimized. In doing so, the symmetry is reduced to $P1$. The optimized lattice parameters of Fe-doped graphite are $a = b = 2.484$ Å, $c = 9.776$ Å, $\alpha = 97.556$, $\beta = 85.339$, and $\gamma = 120.008$. The optimized structure of Fe-doped graphite is shown in Fig. 5, which clearly reveals that the optimized position of Fe is not exactly located between the two graphene layers but is more attracted to one of the graphene sheets as compared to the other. This suggests two different types of graphene layers in iron-doped CNTs, one preferentially doped as compared to the other side of iron. The strong interaction between iron and carbon not only lifts the Fermi level (FL) into the conduction band, it also distorts the π and $\pi^\star$ bands so that they do not remain quasisymmetric around the K point of doped graphene. Thus, as compared to pristine graphene, a different route is followed for the excitation of the D mode via resonant Raman excitation.

Considering that the dimensions of MWCNTs (diameter ~100 nm) are very large, we compare our calculated results of graphite with those of the MWCNTs found in experiments. The undoped electronic band structure and phonon dispersions are presented in Fig. 6 and are used to calculate the Raman shift for the undoped scenario by finding the k values from the electronic band structure for a particular λ_{ex} and finding the corresponding phonon frequency at a corresponding q value measured from the K point of the phonon-dispersion curves. In second-order double-resonance Raman processes (DRRPs) for sp^2 carbon materials (that have linear dispersion around the K point), the electron absorbs a photon at a k state and goes to the conduction band, scatters to a $k + q$ state, scatters back to a k state, and emits a photon by recombining with a hole at a k state. Therefore, in DRRPs, two resonance conditions for three intermediate states should be satisfied in which the intermediate $k + q$ state is always a real electronic state and either the initial or the final k state is a real electronic state.[18] When laser energy is increased, the resonance k vector for the electron moves away from the K point. In double-resonance Raman processes,[18] the corresponding q vector for the phonon changes with increasing k as measured from the K point. Thus, by changing the laser energy, we can observe the phonon energy $\hbar\omega\,(q)$ along the phonon-dispersion relations obtained from first-principles calculations. This is how we eventually

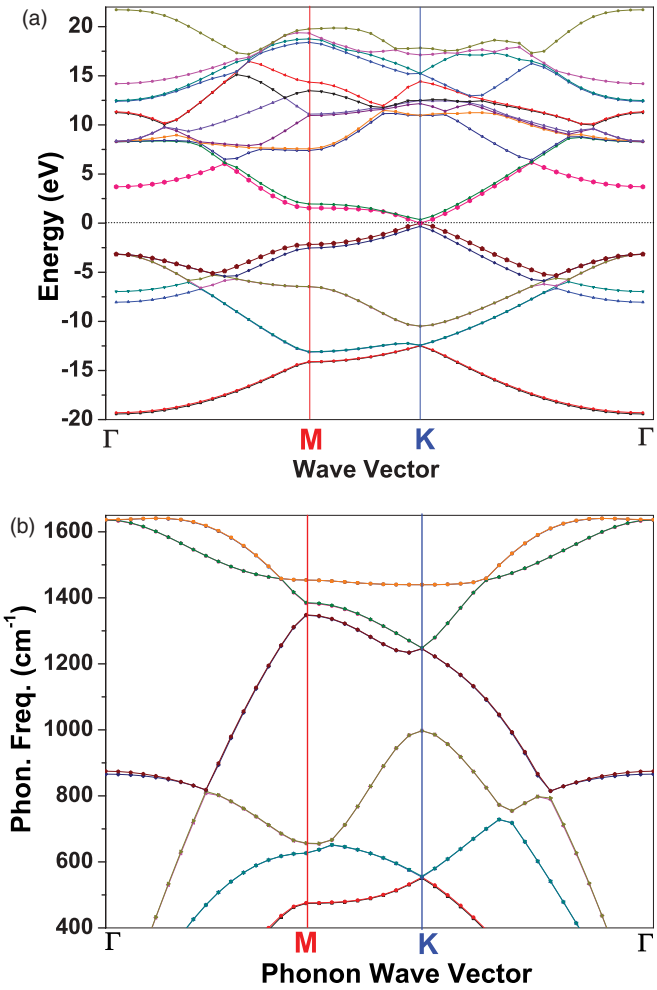

FIG. 6. (Color online) (a) Electronic band structure and (b) phonon dispersion for undoped graphite, respectively.

calculate the Raman shift of the D peak theoretically. The phonon-mode frequencies of graphite have been recently observed by inelastic x-ray scattering,[19,20] and our results agree with those. The phonon-dispersion curve for the D mode has a minima at the K point. The greater the Fe doping, the more distortion is in the electronic band structure compared to the undoped case. This causes drastic changes in the electronic band structure and selects phonons with larger wave vectors. On doping with Fe, a large amount of charge transfer takes place, causing the splitting of various phonon branches around symmetry points [cf. Fig. 7(b)].

IV. DISCUSSIONS

Experimental observations and theoretical calculations of the Raman shift of the D (undoped) and D_1 and D_2 (doped) samples are presented in Fig. 3. The experimental points (represented by symbols without lines) match well with the theoretically determined values (presented by solid lines) within less than 5%. The electronic band structure for Fe-doped graphite is shown in Fig. 7. One can distinguish a much greater number of bands due to doping as compared to the undoped case. We show the lower-energy part of the band structure in Fig. 8. The highest valance band close to the Fermi level

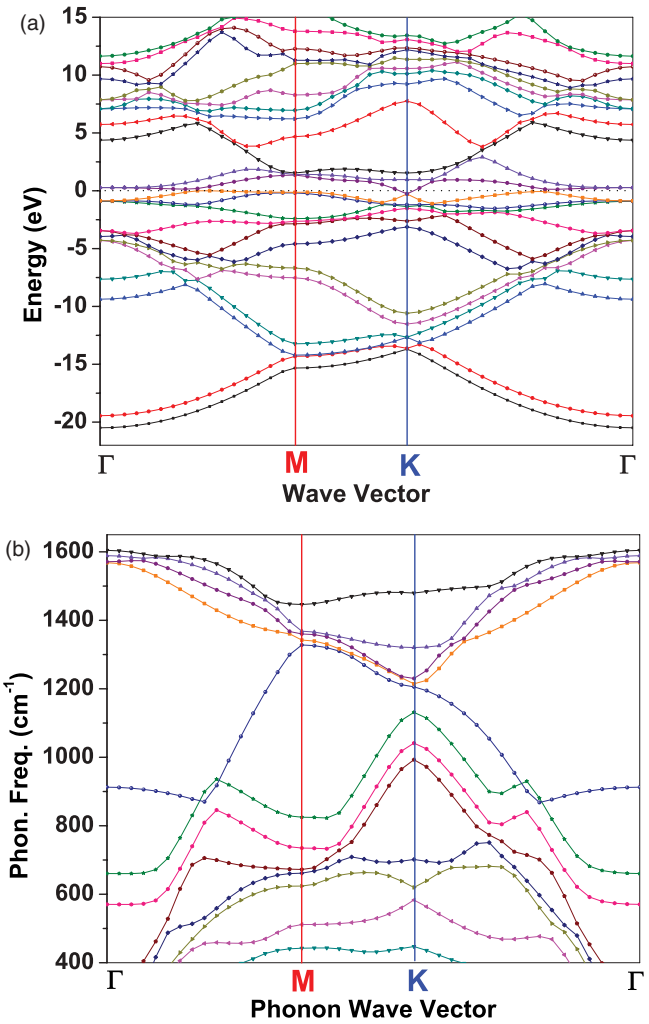

FIG. 7. (Color online) (a) Electronic band structure and (b) phonon dispersion for Fe-doped graphite, respectively. The phonon frequencies are scaled overall by 1% to larger frequencies.

(represented by the dotted line at $E = 0$, cf. Fig. 8) is V-shaped slightly away from the symmetric K point in contrast to that of the undoped electronic band structure. This particular feature, an artifact of doping, gives rise to two k values for the same λ_{ex}. Correspondingly, we get two Raman-active frequencies. One of them shows exactly the same dispersion as that of the undoped case. The other shows stronger dispersion. Thus, the anomalous electronic band structure in the doped case (Fig. 7) is the reason for the splitting of the D peak into D_1 and D_2 that is observed experimentally. These together explain the splitting of the D peak as well as the larger dispersion of the D_1 peak upon doping. It is self-evident from Figs. 5, 7, and 8 that the electronic states at k (with energy ε_k) and $k + q$ (with energy ε_{k+q}) need not belong to the FS that violates the electron-hole symmetry $\varepsilon_k = -\varepsilon_{k+q}$. As a result, the Kohn anomaly is expected to be *weaker* in the doped case. Hence, the dominant mechanism of the red Raman shift and dispersion in the D_1 peak of Fe-doped MWCNTs is due to drastic changes in the electronic band structure caused by strong charge transfer and preferential doping which in turn renormalizes the phonon dispersion. The slopes of the phonon-dispersion curves in the doped case are also very different than those of the undoped

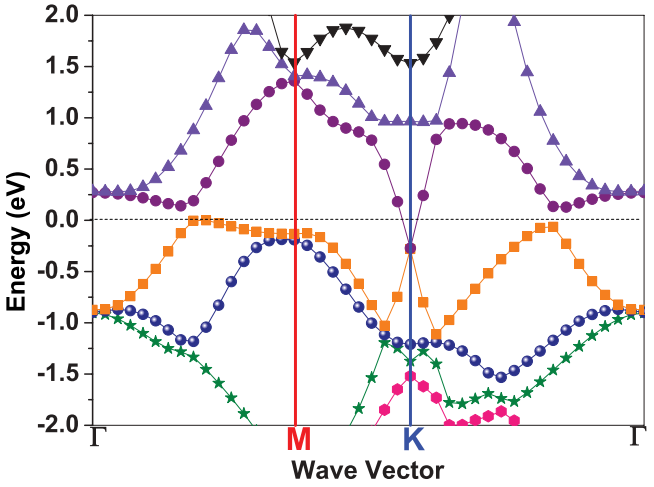

FIG. 8. (Color online) Low-energy electronic band structure of Fe-doped graphite (the same as that of Fig. 7).

case. These together explain the splitting of the D peak as well as the larger dispersion of the D_1 peak on doping.

Given our observations and theoretical understanding when compared with the previous studies carried out in Ref. 6, two major differences are found. The previous studies rely on phonon renormalization due to the Kohn anomaly that further renormalizes electronic bands. Fe doping in MWCNTs clearly weakens the Kohn anomaly as described above. Secondly, doping with substitutional impurities (such as P and N), whose electronic configurations are similar to that of C, becomes part of the SWCNTs whereas for transition metals such as Fe, whose size and electronic configurations are very different from those of C, the above is unlikely. The mechanism of charge transfer, bonding with the host, in the two scenarios is very different. Therefore, further experimental and theoretical understanding is warranted. Raman studies should be carried out on samples doped under identical experimental conditions such as (i) the doping operation on presynthesized MWCNTs (as in our study) and (ii) MWCNTs already grown in the doped condition (as in the previous studies). SWCNTs, DWCNTs, and MWCNTs should be doped with both substitutional impurities as well as with transition metals. We believe that these studies will differentiate between the renormalization of phonons and/or drastic changes in electronic structure issues. The electronic band structures and phonon dispersions should be explicitly calculated through appropriate first-principles methods, and then the calculated Raman shifts should be compared with the observed one. Such an effort is ongoing and will be reported elsewhere.

V. CONCLUSIONS

Therefore, through evidence from the redshifts in the D and G peaks in Raman spectra and the blueshifted component in XPS measurements on doped samples, we conclude that iron doping in MWCNTs acts as a donor. Three effects, namely, the red Raman shift in the D peak we observed (in contrast to the defect-induced blue Raman shift), its splitting into the $D_{1,2}$ peaks, and the larger dispersion of the D_1 peak, are observed. Because of the strong affinity of Fe with carbon,

two alternate, inequivalent graphene sheets are formed (cf. Fig. 5), giving rise to the splitting of the *D* peak. These results are corroborated by the additional prominent peak in the XPS spectra of doped samples. These experimental observations are explained through detailed *ab initio* studies of the electronic and phonon-dispersion calculations. It is shown that the mechanism of the red Raman shift in the *D* peak is electronic in origin, modifying the slope of the phonon dispersions. A semiquantitative agreement between the experimental and theoretical values of the positions and dispersions of the *D* and *G* peaks is obtained. The use of Fe in catalyzing the growth of CNTs is an open problem. We believe our studies will be applicable to newly discovered systems like silicene and will lead to further exciting experimental and theoretical studies of transition-metal doping in MWCNTs.

ACKNOWLEDGMENTS

The authors acknowledge V. Sathe for Raman measurements; D. M. Phase for XPS measurements; and G. Amarendra and P. K. Gupta for discussions. The Brahma cluster was used for computation.

[1]K. S. Novoselov, A. K. Geim, S. V. Morozov, D. Jiang, M. I. Katsnelson, I. V. Grigorieva, S. V. Dubonos, and A. A. Firsov, Nature (London) **438**, 197 (2005).

[2]D. Powell, Science News (Washington, DC) **179**, 14 (2011).

[3]M. Houssa, G. Pourtois, M. M. Heyns, V. V. Afanas'ev, and A. Stesmans, J. Electrochem. Soc. **158**, H107 (2011).

[4]M. S. Dresselhaus, G. Dresselhaus, R. Saito, and A. Jorio, Phys. Rep. **409**, 47 (2005); A. C. Ferrari and J. Robertson, Phys. Rev. B **61**, 14095 (2000); R. Saito, G. Dresselhaus, and M. S. Dresselhaus, in *Physical Properties of Carbon Nanotubes* (Imperial College Press, London, 1998).

[5]S. Costa and E. Borowiak-Palen, Acta Physica Polonica A **116**, 32 (2009); A. C. Ferrari, Solid State Commun. **143**, 47 (2007).

[6]I. O. Maciel, N. Anderson, M. A. Pimenta, A. Hartschuh, H. Qian, M. Terrones, J. Campos-Delgado, A. M. Rao, L. Novotny, and A. Jorio, Nat. Mater. **7**, 878 (2008); I. O. Maciel, J. Campos-Delgado, E. Cruz-Silva, M. A. Pimenta, B. G. Sumpter, V. Meunier, F. López-Urías, E. Muñoz-Sandoval, H. Terrones, M. Terrones, and A. Jorio, Nano Lett. **9**, 2267 (2009); I. O. Maciel, J. Campos-Delgado, M. A. Pimenta, M. Terrones, H. Terrones, A. M. Rao, and A. Jorio, Phys. Status Solidi B **246**, 2432 (2009); J. Campos-Delgado, I. O. Maciel, D. A. Cullen, D. J. Smith, A. Jorio, M. A. Pimenta, H. Terrones, and M. Terrones, ACS Nano **4**, 1696 (2010); M. A. Pimenta, G. Dresselhaus, M. S. Dresselhaus, L. G. Canado, A. Jorio, and R. Saito, Phys. Chem. Chem. Phys. **9**, 1276 (2007), and references therein.

[7]G. M. Bhalerao, A. K. Sinha, H. Srivastava, and A. K. Srivastava, Appl. Phys. A **95**, 373 (2009).

[8]J. Chen, J. Y. Shan, T. Tsukada, F. Munekane, A. Kuno, M. Matsuo, T. Hayashi, Y. A. Kim, and M. Endo, Carbon **45**, 274 (2007); Y. A. Kim, T. Hayashi, K. Osawa, M. S. Dresselhaus, and M. Endo, Chem. Phys. Lett. **380**, 319 (2003); A. C. Ferrari and J. Robertson, Phys. Rev. B **61**, 14095 (2000).

[9]R. P. Vidano, D. B. Fischbach, L. J. Willis, and T. M. Loehr, Solid State Commun. **39**, 341 (1981).

[10]G. M. Bhalerao, A. K. Sinha, and V. Sathe, Phys. E (Amsterdam, Neth.) **41**, 54 (2008).

[11]Y. F. Li, R. Hatakeyama, T. Kaneko, T. Izumida, T. Okada, and T. Kato, Nanotechnology **17**, 4143 (2006).

[12]M. S. Dresselhaus and G. Dresselhaus, Adv. Phys. **51**, 1 (2002).

[13]G. Wertheim, P. M. T. M. Van Attekum, and S. Basu, Solid State Commun. **33**, 1127 (1980); K. Smith and K. M. Black, J. Vac. Sci. Technol. A **2**, 744 (1984).

[14]A. K. Chakraborty, R. A. J. Woolley, Y. V. Butenko, V. R. Dhanak, L. Siller, and M. R. C. Hunt, Carbon **45**, 2744 (2007).

[15]S. B. DiCenzo, G. K. Wertheim, S. Basu, and J. E. Fischer, Phys. Rev. B **24**, 2270 (1981); P. Bennich, C. Puglia, P. A. Bruhwiler, A. Nilsson, A. J. Maxwell, A. Sandell, N. Martensson, and P. Rudolf, *ibid*. **59**, 8292 (1999); S. P. Kelty, Z. Lu, and C. M. Lieber, J. Phys. Chem. **95**, 6754 (1991).

[16]J. M. Soler, E. Artacho, J. D. Gale, A. Garcia, J. Junquera, P. Ordejón, and D. Sánchez-Portal, J. Phys.: Condens. Matter **14**, 2745 (2002).

[17]J. P. Perdew, K. Burke, and M. Ernzerhof, Phys. Rev. Lett. **77**, 3865 (1996).

[18]C. Thomsen and S. Reich, Phys. Rev. Lett. **85**, 5214 (2000).

[19]J. Maultzsch, S. Reich, C. Thomsen, H. Requardt, and P. Ordejon, Phys. Rev. Lett. **92**, 075501 (2004).

[20]M. Mohr, J. Maultzsch, E. Dobardzic, S. Reich, I. Milosevic, M. Damnjanovic, A. Bosak, M. Krisch, and C. Thomsen, Phys. Rev. B **76**, 035439 (2007).